ISSN 1027-5495. Functional Materials, 33, No.3 (2026), p. 553-561
doi:http://dx.doi.org/10.15407/fm33.03.553 © 2026 — SSI "Institute for Single Crystals"
This is an open access article under the CC BY-NC-ND license (http://creativecommons.org/licenses/by-nc-nd/4.0/).

Co_3O_4-doped WO_3 sensor sensitivity to H_2S gas using transition state theory: Predicting optimal doping ratio for maximum sensitivity

Mudar Ahmed Abdulsattar

Ministry of Science and Technology, Baghdad, Iraq
Corresponding author, E-mail: mudarahmed3@yahoo.com

Received February 27, 2026, approved May 05, 2026

Gas sensor science is currently an experimental field and relies only to a small extent on theoretical calculations. However, novel recent advances in theoretical gas sensor models can predict the exact doping ratio for maximum sensitivity and lowest response time. In this work, WO_3 doped with Co_3O_4 is used to monitor colorless, toxic H_2S gas. Combined transition state and density functional theories are employed in the proposed new model to predict and simulate the reaction of H_2S gas with a doped WO_3 sensor. Gibbs free energy is used to assess the stability of the sensor material in an oxygen environment. The number of reactions due to the passage of H_2S gas over the sensor material surface is assumed to be proportional to the sensor response. The variation in sensor response with temperature and H_2S concentration is calculated and compared with experimental results. The theoretically predicted Co/W molar ratio of 0.43 (13 wt% Co_3O_4/WO_3) corresponds to an optimum response very close to the experimental value. H_2S autoignition at temperatures near 250°C limits the measurement procedure to prevent the autoignition temperature from being significantly exceeded. Humidity effects are considered and compared with experiments. Promising new theoretical methods can make theory indispensable in gas sensing research.

Keywords: WO_3 gas sensor; Co_3O_4 doping; H_2S sensor; Density functional theory; Transition state.

Чутливість сенсора WO_3, легованого Co_3O_4, до газоподібного H_2S з використанням теорії перехідного стану: прогнозування оптимального коефіцієнта легування для максимальної чутливості. *Mudar Ahmed Abdulsattar*

Наука про газові сенсори наразі є експериментальною галуззю і лише незначно спирається на теоретичні розрахунки. Однак, останні досягнення в теоретичних моделях газових сенсорів можуть передбачити точний коефіцієнт легування для максимальної чутливості та найменшого часу відгуку. У цій роботі WO_3, легований Co_3O_4, використовується для моніторингу безбарвного, токсичного газоподібного H_2S. У запропонованій новій моделі використовуються комбіновані теорії перехідного стану та функціоналу густини для прогнозування та моделювання реакції газоподібного H_2S з легованим сенсором WO_3. Вільна енергія Гіббса використовується для оцінки стабільності матеріалу сенсора в кисневому середовищі. Вважається, що кількість реакцій, зумовлених проходженням газоподібного H_2S по поверхні матеріалу сенсора, пропорційна відгуку сенсора. Розраховано зміну реакції сенсора залежно від температури та концентрації H_2S та порівняно з експериментальними результатами. Теоретично передбачене молярне співвідношення Co/W=0,43 (13 мас.% Co_3O_4/WO_3) відповідає оптимальній реакції, дуже близької до експериментального значення. Самозаймання H_2S за температур поблизу 250 °C обмежує процедуру вимірювання для запобігання перевищення температури самозаймання. Розглянуто вплив вологості та порівняно з експериментальними результатами. Перспективні нові теоретичні методи можуть зробити теорію незамінною в дослідженнях газового сенсора.

1. Introduction

WO_3 is one of the preferred gas sensors for detecting reducing gases such as methane, ethane, H_2, and CO [1, 2]. These gases remove or replace oxygen from the sensor material. Since WO_3 has a high number of oxygen atoms, it is ideal for sensor analysis of reducing gases. However, picking oxygen from WO_3 requires relatively high energy. This energy can be reduced by doping with other metal oxides containing fewer oxygen atoms, such as PdO [3], ZnO [4], and Co_3O_4 [5].

Co_3O_4 is a mixed oxide of two cobalt oxides ($CoO.Co_2O_3$). Co_3O_4 is used as a gas-sensing material for many gases, such as ethanol [6], ammonia [7], and acetone [8]. Co and its oxides are known to be efficient catalysts [9]. Cobalt, being a transition metal and having several oxidation states, has basic catalytic properties. Co_3O_4 is a low-cost, abundant oxide, making it well-suited for gas sensors. WO_3 is an *n*-type semiconductor [10] while Co_3O_4 is a *p*-type semiconductor [11] that is combined to form a *p-n* junction.

Hydrogen sulfide is a toxic gas that originates from the decomposition of organic compounds, industrial activities, petroleum processing, and other natural and artificial sources [12,13]. In most cases, maximum permissible concentrations in the workplace should not exceed 20 ppm [14]. H_2S properties, such as colorlessness, toxicity and flammability are the main reasons for the need to detect this gas [15]. The autoignition temperature of H_2S is around 250°C, while the flash point temperature is about 82.4°C [16]. As a result, H_2S cannot be detected as a gas at temperatures less than 82.4°C since there is not enough gas vapor at temperatures below this temperature. It cannot be detected far above 250°C since the concentration decreases rapidly after this temperature.

Density functional theory (DFT) is a tool that has proven useful in many areas of science, including current gas sensor theory. However, to fully realize the benefits of DFT in gas sensors, reaction rate theories should be combined with DFT. Gas sensing is essentially a reaction between the censored gas and the sensing material. The reaction rate can be calculated using several theories, such as transition state theory (TST) [17] and the Arrhenius equation [18]. TST has been well established for thermodynamic quantities, such as Gibbs energy, enthalpy, and transition entropy, which promote its use in gas sensing.

In this work, a Co_3O_4/WO_3 composite is used to detect H_2S gas. The optimal doping ratio for maximum sensitivity is first predicted and compared with the experimental results. Thermodynamic quantities of the transition state are evaluated, including the Gibbs free energy of transition. The reaction rate is calculated, and the number of reactions is correlated with the sensor response. The sensor response and response time are evaluated as a function of temperature and H_2S concentration. The autoignition temperature of H_2S is considered crucial to determine the maximum sensitivity temperature. The effect of humidity and long-term stability is discussed. The selectivity of the sensor for various gases relative to H_2S is also shown as a function of temperature.

2. Theory

In the present work, density functional theory is used with the Gaussian 09 software package [10], including its graphical interface GaussView 5.0. The DFT calculations include structural optimization, transition-state calculations, and the evaluation of thermodynamic quantities, including Gibbs free energy, enthalpy, and entropy. The B3LYP method is used because of its success in gas-sensor calculations [19]. 6-311G** basis set is used for light atoms (O, H, S). SDD (Stuttgart/Dresden) basis sets are used for heavier atoms (W, Co). Dispersion correction is mandatory in gas-sensor calculations, since gas reactions are typically long-range [20]. The GD3BJ dispersion correction available in Gaussian 09 was adopted due to its success in previous sensing calculations [21]. Basis-set superposition correction is not added in harmony with previous gas sensor calculations [21].

The use of cluster calculations in gas sensors is a fruitful and successful method [22,23]. In the present work, a doped W_4O_{12} cluster [24] will be used to detect H_2S. The W_4O_{12} cluster is stable in an oxygen environment since it is energetically unfavorable to accept or lose oxygen atoms (all reactions are near standard conditions: 1 atm pressure, 25°C unless mentioned otherwise):

$$W_4O_{12}+½O_2 \rightarrow W_4O_{13}\ (\Delta G=1.584\ eV) \quad (1)$$

$$W_4O_{12} \rightarrow W_4O_{11}+½O_2\ (\Delta G=3.679\ eV) \quad (2)$$

In the above equations, the positive value of the change in the Gibbs free energy of reaction (ΔG) prevents the reactions from occurring.

The above results agree with the fact that 6 is the main oxidation state of tungsten. The W_4O_{12} cluster reacts weakly with H_2S gas as in the replacement reaction:

$$W_4O_{12}+H_2S\rightarrow W_4O_{11}S+H_2O \quad (\Delta G = -0.0107 \text{ eV}) \tag{3}$$

The negative sign of ΔG ensures a slow reaction of W_4O_{12} with H_2S because of the small negative value of ΔG in this reaction at room temperature. The reason for this weak reaction is that the extraction of oxygen from W_4O_{12} requires 3.679 eV, as shown in Eq. (2). To overcome this problem, tungsten oxide is doped with a lower-oxidation-state metal, such as cobalt, in the present work. When one atom of cobalt replaces tungsten in W_4O_{12}, the stable cluster is CoW_3O_{10}. The stability of the formed cluster in an oxygen environment is as follows:

$$CoW_3O_{10}+½O_2\rightarrow CoW_3O_{11} \ (\Delta G=0.575 \text{ eV}) \tag{4}$$

$$CoW_3O_{10}\rightarrow CoW_3O_9+½O_2 \ (\Delta G=2.679 \text{ eV}) \tag{5}$$

Comparing Eq. (4) with Eq. (2), one can notice that there is a reduction in the energy needed to pull oxygen from the doped cluster. This doping property will be used in the next section to determine the doping percentage with the lowest oxygen extraction energy.

In TST, the W_4O_{12} cluster reaction rate with H_2S gas can be given by the equation [25]:

$$\frac{d[W_4O_{12}]}{dt} = -[W_4O_{12}]^u [H_2S]_e^v \ k(T), \tag{6}$$

$$k(T) = A \ T^m \ \exp^{\left(\frac{-\Delta G^!}{k_B T}\right)}. \tag{7}$$

In the above equations, $[W_4O_{12}]$ and $[H_2S]$ are the concentrations of W_4O_{12} clusters and H_2S gas, respectively. The concentration exponents (*u, v*) are empirical parameters that usually take the value 1 for small concentration changes. However, at higher concentrations, *v* takes values in the range (½ to 2), as shall be seen later [26,27]. The subscript (e) in the H_2S gas concentration indicates that the effective concentration of H_2S will decrease as the autoignition temperature reaches about 250 °C:

$$(3/2) \ O_2+H_2S\rightarrow H_2O+SO_2 \ (\Delta G=-3.269 \text{ eV}) \tag{8}$$

The H_2S concentration also decreases due to humidity, since H_2S cannot come into contact with the sensor surface and dissolves in water. The following logistic functions can give the effective concentration of H_2S:

$$[H_2S]_e = [H_2S] - \frac{[H_2S]}{1+e^{k_s(T-T_0)}} \times \frac{1}{1+e^{k_h(h-h_0)}} \tag{9}$$

In the above equation, k_s and k_h are the rates at which H_2S gas decreases due to autoignition and humidity, respectively. T_0 and h_0 are the temperature and humidity at which H_2S concentration reaches its half value due to autoignition and humidity, respectively.

The final step is to determine the number of reactions involving W_4O_{12} clusters and H_2S gas. The number of reactions is assumed to be proportional to the change in the sensor response caused by the presence of H_2S gas. To obtain the number of reactions within a period (response time (t_{res})), Eq. (6) should be integrated:

$$\int d[W_4O_{12}] = -\int [W_4O_{12}]^u [H_2S]_e^v \ k(T) dt, \tag{10}$$

$$\int d[W_4O_{11}S] = -\int d[W_4O_{12}] = \\ = \int [W_4O_{12}]^u [H_2S]_e^v \ k(T) dt, \tag{11}$$

$$[W_4O_{11}S] = C + [W_4O_{12}]^u [H_2S]_e^v \ k(T) t_{res}, \tag{12}$$

In the above equations, the decrease in the concentration of the W_4O_{12} clusters ($d[W_4O_{12}]$) corresponds to an increase in the sulfurized clusters ($-d[W_4O_{11}S]$) as in Eq. (3). The response is assumed to be proportional to the concentration of formed $W_4O_{11}S$ clusters [25]:

$$\text{Response} = \frac{R_a}{R_g} = \\ = 1 + c[W_4O_{12}]^u [H_2S]_e^v \ k(T), \tag{13}$$

The experimental response for reducing gases is the ratio of the resistance in pure air (R_a) to the resistance at a specific H_2S concentration (R_g). In the above equation, the constant is equal to 1 because the experimental response is equal to one when the concentration of the detected gas vanishes. The same equations hold for the doped clusters.

3. Results and discussion

Fig. 1 shows both the adsorption (a) and transition (b) states of H_2S on doped cluster CoW_3O_{10}. Although the two figures (a and b) seem similar, Fig. 1a has the S atom relatively nearer to the Co atoms, while the two H atoms are relatively far from the O atoms as compared to Fig. 1b. Using Natural Bond Order (NBO) analysis, we find that both Co and H atoms have positive charges, while both S and O atoms have nega-

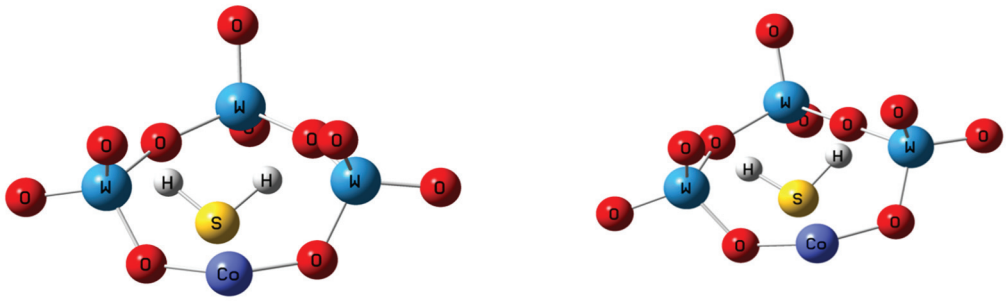

a b

Fig. 1. (a) Geometrical optimization of H_2S adsorption on CoW_3O_{10} cluster. (b) The transition state of H_2S on the CoW_3O_{10} cluster.

tive charges. As a result, the adsorption state has a lower energy than the transition state. The adsorption energies of H_2S on W_4O_{12} and CoW_3O_{11} clusters are -0.183 and -1.045 eV, respectively. This large difference between the original and doped clusters indicates a stronger interaction between H_2S and the doped cluster.

Fig. 2 shows the variation of the transition state between H_2S and Co-doped W_4O_{12} clusters as a function of temperature. The transition state of the original W_4O_{12} cluster with H_2S gas is also shown. Surprisingly, the transition states of the doped and undoped materials intersect at almost the highest response temperature, as will be shown later. The highest response temperature is also near the H_2S autoignition temperature. The Gibbs transition state energy ($G^{‡}$) of undoped WO_3 increases with temperature, while the transition state energy of doped clusters begins to decrease at high doping ratios due to the positive transition entropy ($S^{‡}$) and nearly constant enthalpy ($H^{‡}$), as in the equation:

$$G^{‡} = H^{‡} - TS^{‡} \quad (15)$$

Fig. 3 shows the variation of the Gibbs energy of oxygen reduction of Co-doped WO_3 as a function of the Co/W molar ratio. Two experimental molar ratios are shown [5]. Peak 1 is the experimentally observed peak with the highest response factor at a molar ratio of 0.33, while peak 2 is the second-highest at a molar ratio of 0.5. Due to the limited number of experimental trials, peak 1 is selected as the optimal molar ratio for the highest response [5]. However, Fig. 3 has another theoretical peak at a molar ratio of 0.43 (13 wt% Co_3O_4/WO_3). This theoretical peak was chosen taking into account the following considerations. The energy of ideal gas particles (3/2 k_BT) at room temperature is

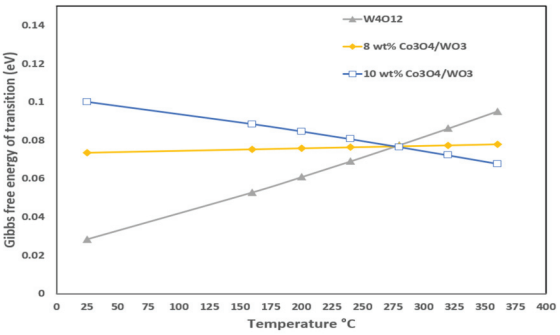

Fig. 2. Gibbs energy of transition of H_2S at different contents Co_3O_4/WO_3 (wt%) as a function of temperature.

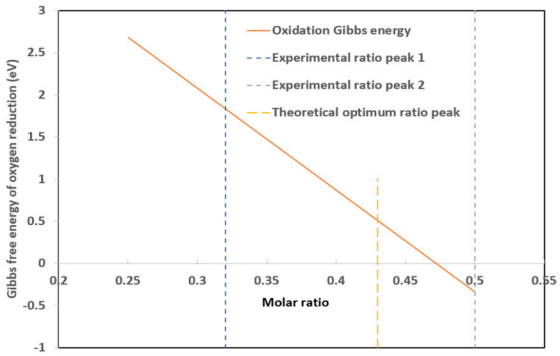

Fig. 3. Gibbs energy of oxygen reduction of Co_3O_4/WO_3 as a function of the Co/W molar ratio at room temperature. The optimum experimental [5] and theoretical ratios are shown.

approximately 0.04 eV. At gas sensor working temperatures of 250°C, this energy reaches approximately 0.07 eV. To account for multiple collisions of atmospheric gases with the sensor material, this number can be multiplied by factors that ensure chemical stability. Generally, 0.5 eV is sufficient to maintain stability, compared to the experimentally chosen 1.7 eV for peak 1 [5]. Peak 2 has a negative Gibbs energy, which will cause the sensor to lose some oxygen to the surrounding atmosphere even before the sensing procedure begins. Sadly, this method

Table 1. Response parameters of the 10 wt%Co_3O_4/WO_3 sensor to H_2S. Gibbs free energy of activation ($\Delta G^{‡}$) at 25°C and 1 bar.

Reaction	$\Delta G^{‡}$ (eV)	A ($s^{-1}. K^{-6}$)	m	v,u	k_s ($°C^{-1}$)	T_0 (°C)	k_h	h_0 (%)	c (s)
[10 wt%Co_3O_4/WO_3---H_2S]^a ↓ [10 wt%Co_3O_4/WO_3---H_2S]‡	0.100	2.0×10-11	6	1	0.03	290	0.06	67	19

is not used by experimentalists, although it reduces the effort, time, and cost of finding the precise point of maximum sensitivity. The theoretically chosen molar ratio yields the highest responses and the lowest response time compared to the experimentally chosen ratio.

Table 1 lists the parameters used to simulate the interaction between H_2S gas and 10 wt% Co_3O_4/WO_3. The adsorption and transition states are assigned as [10 wt%Co_3O_4/WO_3---H_2S]^a and [10 wt%Co_3O_4/WO_3---H_2S]‡, respectively. The Gibbs energy of activation, or transition, is only 0.1 eV, which is small compared to conventional activation energies [28]. The activation energy is calculated using the transition-state (t_s) optimization option in Gaussian [29].

The pre-exponential factor (A) in Eq. (7) is a fitting parameter that reflects the properties of the sensor material, such as surface area, chemical composition, crystalline properties, doping, oxidation, etc. The value of this parameter (Table 1) in the present case is 2.0×10^{-11} $s^{-1}. K^{-6}$. This value is close to the sensitivity of MnO_2-doped MoO_3 to H_2S gas [16]. The similarity between MoO_3 and WO_3 in their oxidation states might be the origin of the convergence in the A parameter values.

The temperature exponent parameter (m) in Table 1 is 6. The (m) parameter varies in the range of (0-12). The original value of this parameter in the Arrhenius equation is (0) [30]. However, the original transition state theory gave this parameter the value of (1) [31]. Practically, to fit the experimental data, the value of this parameter can reach (12) [25]. The present value (6) is the average of this range (0-12).

The concentration exponent parameters (u, v) have the value of (1). This value is assigned to the exponent for small changes in concentration, as illustrated in Fig. 5 below. For wider concentration ranges, the v exponent can take values from ½ to 2, with a decrease or increase in response at higher concentration values, respectively.

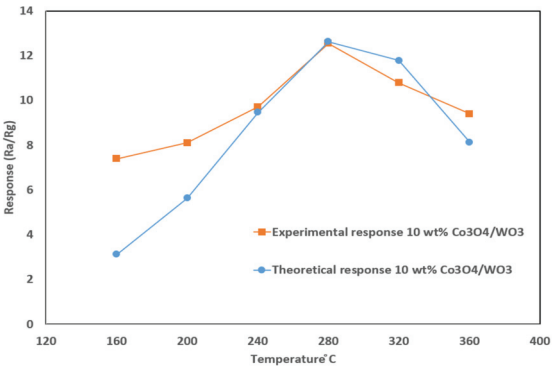

Fig. 4. Experimental [5] and theoretical variation of sensor response to 10 ppm H_2S gas as a function of temperature for a 10 wt% Co_3O_4/WO_3 sensor at low humidity.

The autoignition and humidity parameters (k_s, T_0, k_h, and h_0) are expressed as logistic functions, which have many applications in physics and chemistry [32]. The T_0 parameter is close to the H_2S autoignition temperature at 250°C, while h_0 is close to the humidity level that has a significant effect on response at 67% relative humidity. The rate of response reduction due to autoignition and humidity (k_s, k_h respectively) is relatively small at the values $0.03°C^{-1}$ and 0.06 respectively.

The correlation parameter (c) between the response and the concentration of the H_2S reaction product with the censor material is 19 s. This value is lower than that of previous gas sensor materials [16]. The low value can be understood from the discussion in Fig. 3, since the experimentally chosen doping ratio (Co/W) does not correspond to the optimal response99.

Fig. 4 shows the experimental and theoretical variations in sensor response to 10 ppm H_2S gas as a function of temperature for the 10 wt% Co_3O_4/WO_3 sensor. Acceptable agreement is observed between theory and experiment except at the temperature range 150-200°C. Both experimental and theoretical curves peak at 280 °C. After 280°C, the response slows down due to the decrease in the

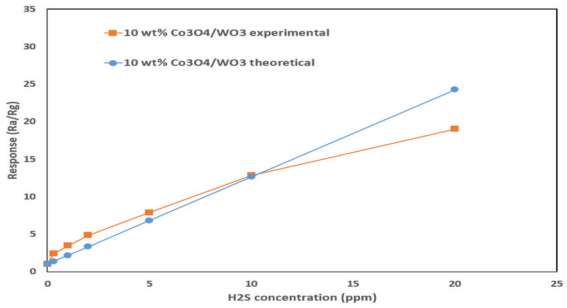

Fig. 5. the variation of experimental [5] and theoretical response for a 10 wt% Co_3O_4/WO_3 sensor as a function of H_2S concentration at 280°C and low humidity.

H_2S concentration as a result of autoignition. The maximum response temperatures of pure Co_3O_4, WO_3, or their combination are all in the range 240-280°C, indicating that the maximum response is approximately independent of the sensor material but dependent on the detected gas and its autoignition temperature [5].

Fig. 5 shows the variation of experimental and theoretical response for the sensor 10 wt% Co_3O_4/WO_3 as a function of H_2S concentration at 280°C. Acceptable agreement is observed in the low concentration range (0-15 ppm) of H_2S. Higher H_2S concentration requires the use of an H_2S concentration exponent that is less than 1, as discussed in the theory section [26].

Fig. 6 shows the theoretical 90% response time ($t_{res(90\%)}$) as a function of temperature compared to the experiment of H_2S gas with a 10 wt% Co_3O_4/WO_3 sensor at 280°C and low humidity. The 90% response time is the time required to reach 90% of the final resistance after gas exposure. This time can be obtained from Eq. (6):

$$t_{res(90\%)} = \frac{\ln(10)}{[H_2S]_e^{v} A T^{m} \exp\left(\frac{-\Delta G^{!}}{k_B T}\right)}. \qquad (11)$$

$t_{res(90\%)}$ reaches its minimum value at the maximum response at 280°C at low humidity. Good agreement between theory and experiment is obtained.

Fig. 7 shows the effect of humidity on the sensor response. Humidity affects the sensor's chemical composition, reducing the number of reactions between H_2S gas and the sensor material. H_2O molecules create an additional barrier on the sensor surface, preventing some reactions from occurring. In addition, H_2S dissolves in water molecules, forming a weak acid that further weakens its reaction. Fig. 7 shows that the response reaches half its value at 67% humidity.

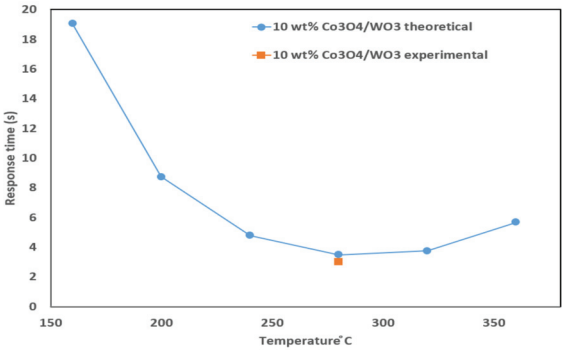

Fig. 6. Theoretical 90% response time ($t_{res(90\%)}$) as a function of temperature compared to the experiment [5] of 10 ppm H_2S gas with a 10 wt% Co_3O_4/WO_3 sensor at 280 °C and low humidity.

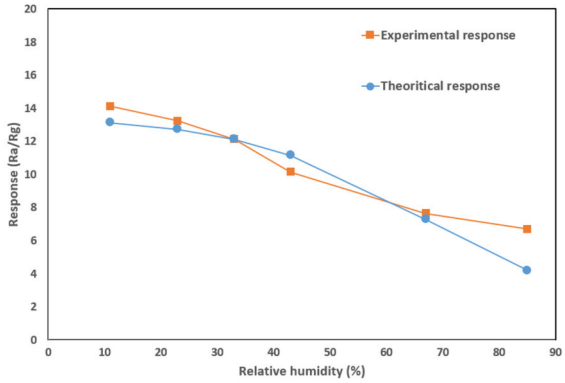

Fig. 7. Theoretical effect of relative humidity on the sensor response of 10 ppm H_2S gas with a 10 wt% Co_3O_4/WO_3 sensor at 280°C compared to experiment [5].

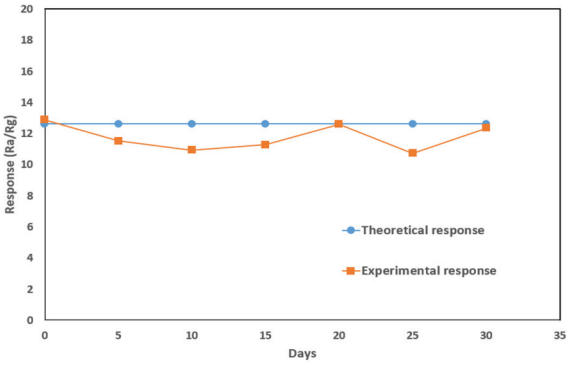

Fig. 8. Theoretical response of a10 wt% Co_3O_4/WO_3 sensor for 30 days to 10 ppm of H_2S gas at 280°C temperature compared to experiment [5].

Fig. 8 shows 30 days of a 10 wt% Co_3O_4/WO_3 sensor response to 10 ppm of H_2S gas at 280°C. After the initial calibration, the sensor response decreases due to humidity, dust, contamination, degradation, and aging. As a result, the sensor needs to be recalibrated after a reasonable period to restore correct monitoring. Humidity fluctuations can be overcome by measuring the response and humidity simultaneously and correcting for humidity changes.

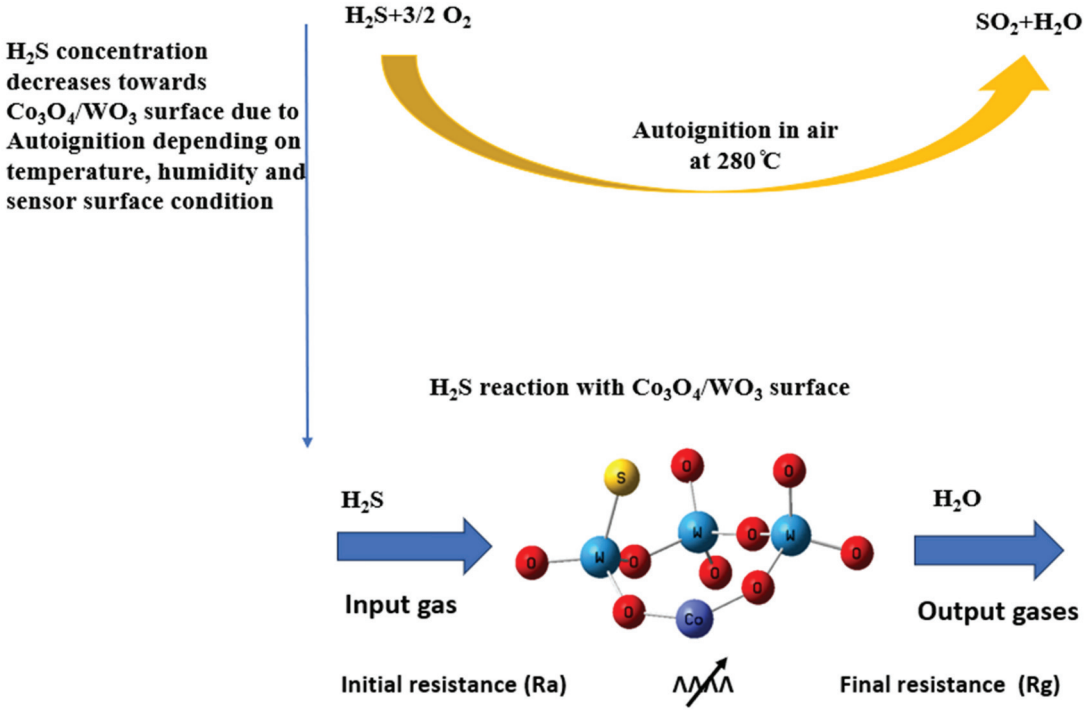

Fig. 9. A summary of reactions discussed in the present work. First (upper part of figure): the reaction of H_2S with oxygen in air at temperatures near the autoignition temperature. Below (lower part of the figure): the reaction of H_2S with the sensor material that finally changes the sensor resistance.

Fig. 9 summarizes the reactions discussed in the present work. First, the reaction of H_2S with oxygen in the air at temperatures near the autoignition temperature is considered. Replacing oxygen atoms with sulfur atoms at the sensor surface changes the sensor's resistivity, indicating the presence of H_2S molecules. The initial resistance in pure air (R_a) is adjusted to the final resistance (R_g) based on the H_2S gas concentration. Note that GaussView uses default bond distance thresholds for specific elements. If the calculated sulfur-metal bond distance is longer than the default threshold for a double bond, GaussView renders it as a single bond for visualization purposes only as in Fig. 9.

The autoignition temperatures of different gases can be used to differentiate them by evaluating their temperature sensitivity. Every gas has an intrinsic autoignition temperature, such as ethane, methane, and methanol [33]. As an example, the alkanes have an autoignition temperature range from 450 to 850°C depending on the hydrocarbon chain length. The same is true for cycloalkanes, alcohols, etc. [33].

4. Conclusions

Theoretical analysis of sensor response can reveal many important features of gas sensing and the materials used in sensing processes. The transition-state theory combined with density functional theory and cluster formalism can reproduce the experimental data on sensor response as a function of temperature and gas concentration. H_2S gas was detected using a Co_3O_4-doped WO_3 sensor, which showed an optimum sensitivity at a theoretical molar ratio of Co/W = 0.43 (13 wt% Co_3O_4/WO_3) very close to experimental results. This optimal Co/W molar ratio can be used to manufacture high-response sensors. Cobalt doping can result in oxygen atoms being more energetically released to oxidize H_2S gas compared to pure WO_3. The variation of Gibbs transition energy with temperature is used to obtain the gas response (R_a/R_g) and response time with temperature. The response to H_2S gas concentration is nearly linear at low concentrations. The shortest response time as a function of temperature corresponds to the maximum response temperature. The effect of relative humidity on response is evaluated using a logistic function similar to that used to simulate the autoignition temperature effect. The sensor is usually recalibrated after a period (months) due to the various effects of humidity, dust, contamination, degradation, aging, etc. The empirical parameters of the present sensor are close to those of previously investigated sensors. The autoignition temperatures of different gases can be used to differentiate them by evaluating their temperature sensitivity.

References

1. J. Wei, Y.-B. Zhang, Y. Li, X.-C. Tang, Z.-H. Qiao, S.-S. Lu, J.-J. Shao, J.-W. Lee, S.-J. Yang, M. Zhao, J.-M. Oh, C. Wang, Y. Li, Ultra-sensitive hydrogen sensor based on powder aerosol deposited WO3 with amorphous matrix encapsulated nanocrystalline, Sensors and Actuators B: Chemical. 452 (2026). https://doi.org/10.1016/j.snb.2025.139420.
2. M. Hu, J. Yu, R. Qin, J. Hu, J. Xu, H.-J. Li, H. Xu, J. Chen, D. Wang, PtPd/CeO2 catalytic enhanced WO3 nanofibers bilayer gas sensor for ppb-level xylene detection, Journal of Hazardous Materials. 501 (2026). https://doi.org/10.1016/j.jhazmat.2025.140742.
3. X. Wang, W. Han, J. Yang, P. Cheng, Y. Wang, C. Feng, C. Wang, H. Zhang, Y. Sun, G. Lu, Conductometric ppb-level triethylamine sensor based on macroporous WO3-W18O49 heterostructures functionalized with carbon layers and PdO nanoparticles, Sensors and Actuators B: Chemical. 361 (2022). https://doi.org/10.1016/j.snb.2022.131707.
4. M. Du, M.I. Abdulraheem, L. Xu, Y. Zang, Y. Song, M.A. Tarighat, V. Raghavan, J. Hu, Enhanced Selectivity Electronic Nose Systems for Agricultural Ammonia Gas Detection via a co-designed WO3-ZnO Sensor Array and Convolutional Neural Networks, Scientific Reports. 15 (2025). https://doi.org/10.1038/s41598-025-26084-z.
5. X. Niu, H. Zhang, J. Zhai, G. Jiao, Z. Ding, D. Zhang, A fast response hydrogen sulfide gas sensor based on Co3O4 and WO3 heterojunction, Sensors and Actuators B: Chemical. 444 (2025). https://doi.org/10.1016/j.snb.2025.138336.
6. Y. Tian, J. Wang, J. Wang, J. Luo, Z. Zou, D. Li, C. Suo, Y. Li, X. Jin, M. Peng, X. Chen, High-performance ethanol gas sensor based on stepped and hollow ZnSnO3/Co3O4 heterostructures, Chemical Engineering Journal. 531 (2026). https://doi.org/10.1016/j.cej.2026.174092.
7. Y. Qin, Y. Zhang, J. Lei, X. Liu, Optimized PANI@SnO2-Co3O4 ammonia sensor with UV/humidity-modulated response and machine learning-assisted early prediction, Sensors and Actuators B: Chemical. 449 (2026). https://doi.org/10.1016/j.snb.2025.139171.
8. L. Li, Q. Diao, Z. Liu, G. Zhu, M. Jiao, C. Liu, M. Du, Y. Shi, Y. Wang, P. Cheng, X. Xu, Preparation of Co3O4 by tunable oxygen defect engineering and its application in acetone gas sensor, Microchemical Journal. 212 (2025). https://doi.org/10.1016/j.microc.2025.113481.
9. W. Tang, J.-P. Cao, X.-Y. Zhao, D. Xie, K.-R. Luan, C.-J. Li, Q.-M. She, T. Bold, Relationship of catalytic performance and catalyst structure evolution based on pressurized CH4-CO2 reforming reaction over carbon-supported Co-Ir alloy catalysts, Fuel. 414 (2026). https://doi.org/10.1016/j.fuel.2026.138320.
10. K. Mitsui, S. Imada, S. Inoué, G. Tricot, K. Ben Tayeb, H. Vezin, M. Mori, T. Katase, H. Hiramatsu, A. Saitoh, Degenerate n-type electrical conductivity in WO3–P2O5 glasses with embedded WO3 nanocrystals, Journal of Physics and Chemistry of Solids. 211 (2026). https://doi.org/10.1016/j.jpcs.2025.113464.
11. G. Li, L. Qian, M. Li, D. Wang, L. Yang, R.-F. Huang, Hollow double-shell Co3O4@CoNiSx p-n heterojunction for enhanced visible light-assisted methanol electrocatalytic oxidation, Electrochimica Acta. 536 (2025). https://doi.org/10.1016/j.electacta.2025.146735.
12. N. Kwak, S. Tsameret, B. Mc Intyre, M. Sobhanian, D. Diaz-Brunet, C. Bi, H. Solo-Gabriele, J. Li, Quantification of sulfur compound emissions from Sargassum Strandings, Marine Pollution Bulletin. 225 (2026). https://doi.org/10.1016/j.marpolbul.2026.119262.
13. M. Gao, J. Liu, Y. Chen, Z. Huang, H. Wang, P. Yuan, X. Xu, J. Yang, Intensification of Multiphase Reactions in Petroleum Processing: A Simulation Study of SK Static Mixer Using NaClO for H2S Removal, Processes. 13 (2025). https://doi.org/10.3390/pr13051515.
14. M. Akbari-Saatlu, M. Schalk, S. Pokhrel, C. Mattsson, L. Madler, M. Procek, H.H. Radamson, G. Thungstrom, Ultrasensitive H2S and CH3SH Sensors Based on SnO2 Porous Structures Utilizing Combination of Flame and Ultrasonic Spray Pyrolysis Methods, IEEE Sensors Journal. 24 (2024) 36393–36402. https://doi.org/10.1109/JSEN.2024.3467168.
15. H. Feng, S. Guo, Y. Guo, Q. Zhao, Y. Xia, Z. Duan, M. Hou, L. Yang, L. Gao, H. Tai, Advances in metal-organic framework-based hydrogen sulfide gas sensors, Coordination Chemistry Reviews. 546 (2026). https://doi.org/10.1016/j.ccr.2025.217087.
16. M.A. Abdulsattar, H2S Properties, temperature, and humidity effects on MnO2 doped MoO3 gas sensor response: Transition state theory study, Ionics. 31 (2025) 8487–8497. https://doi.org/10.1007/s11581-025-06501-z.
17. S. Vari, C. de Falco, C. Cavallotti, NN-VRCTST: Neural Network Potentials Meet Variable Reaction Coordinate Transition State Theory for the Rate Constant Determination of Barrierless Re-

actions, Journal of Chemical Theory and Computation. 21 (2025) 10373–10384. https://doi.org/10.1021/acs.jctc.5c01288.
18. Y. Chung, W.H. Green, New modified Arrhenius equation to describe the temperature dependence of liquid phase reaction rates, Chemical Engineering Journal. 516 (2025). https://doi.org/10.1016/j.cej.2025.163300.
19. L.K. Saini, M. Pandey, Quantum chemical calculation of cyanogen gas sensitivity: Unveiling the high-sensitivity ZnTCPP–C2N2 interaction, Journal of Molecular Modeling. 32 (2026). https://doi.org/10.1007/s00894-025-06612-4.
20. S. Arshadi, M. Salary, O. Marvi, First-principles design of a Mg-porphyrin nanoring sensor via dipole moment and dispersion energy engineering for high-sensitivity detection of hazardous industrial gases, Journal of Molecular Graphics and Modelling. 143 (2026). https://doi.org/10.1016/j.jmgm.2025.109233.
21. V. Moeini, A. Hossein Masoudi Gazi, Doped BC2NNTs with gallium: A new sensor to detect the presence of ozone gas in the gaseous environment, Computational and Theoretical Chemistry. 1235 (2024). https://doi.org/10.1016/j.comptc.2024.114578.
22. R. Molavi, R. Safaiee, M.H. Sheikhi, Oxygen adsorption properties of small cobalt oxide clusters: Application feasibility as oxygen gas sensors, Physical Chemistry Chemical Physics. 22 (2020) 14889–14899. https://doi.org/10.1039/d0cp01951h.
23. H. Liu, W. Shen, X. Chen, J.-P. Corriou, A high-performance NH3 gas sensor based on TiO2 quantum dot clusters with ppb level detection limit at room temperature, Journal of Materials Science: Materials in Electronics. 29 (2018) 18380–18387. https://doi.org/10.1007/s10854-018-9952-9.
24. Y. Zhang, J. Jiang, Y. Liu, P. Li, Y. Liu, L. Chen, J. Zhao, Multi-praseodymium-and-tungsten bridging octameric tellurotungstate and its 2D honeycomb composite film for detecting estrogen, Nanoscale. 12 (2020) 10842–10853. https://doi.org/10.1039/d0nr01901a.
25. M.A. Abdulsattar, WO3 Doped SnS2 Gas Sensor Response to NO2: Effect of Temperature and Humidity Using Transition State Theory Formalism, Eurasian Journal of Chemistry. 30 (2025) 34–44. https://doi.org/https://doi.org/10.31489/2959-0663/4-25-5.
26. M.A. Abdulsattar, R.H. Jabbar, M.A. Al-Seady, Ethanol properties effects on its reaction with Mo-doped SnO2 clusters: A gas sensor model, Results in Surfaces and Interfaces. 17 (2024). https://doi.org/10.1016/j.rsurfi.2024.100291.
27. M.A. Abdulsattar, H.M. Almaroof, W.J. Al-Saraf, Cl2 gas properties, temperature, and humidity effects on SnO2 sensor response: transition state theory study, Journal of Molecular Modeling. 31 (2025). https://doi.org/10.1007/s00894-025-06368-x.
28. A.L. Petrou, The Free Energy of Activation as the critical factor in geochemical processes, Chemical Geology. 308–309 (2012) 50–59. https://doi.org/10.1016/j.chemgeo.2012.03.015.
29. M.J. Frisch, G.W. Trucks, H.B. Schlegel, G.E. Scuseria, M.A. Robb, J.R. Cheeseman, G. Scalmani, V. Barone, B. Mennucci, G.A. Petersson, H. Nakatsuji, M. Caricato, X. Li, H.P. Hratchian, A.F. Izmaylov, J. Bloino, G. Zheng, J.L. Sonnenberg, M. Hada, M. Ehara, K. Toyota, R. Fukuda, J. Hasegawa, M. Ishida, T. Nakajima, Y. Honda, O. Kitao, H. Nakai, T. Vreven, J.A.J. Montgomery, J.E. Peralta, F. Ogliaro, M. Bearpark, J.J. Heyd, E. Brothers, K.N. Kudin, V.N. Staroverov, R. Kobayashi, J. Normand, K. Raghavachari, A. Rendell, J.C. Burant, S.S. Iyengar, J. Tomasi, M. Cossi, N. Rega, J.M. Millam, M. Klene, J.E. Knox, J.B. Cross, V. Bakken, C. Adamo, J. Jaramillo, R. Gomperts, R.E. Stratmann, O. Yazyev, A.J. Austin, R. Cammi, C. Pomelli, J.W. Ochterski, R.L. Martin, K. Morokuma, V.G. Zakrzewski, G.A. Voth, P. Salvador, J.J. Dannenberg, S. Dapprich, A.D. Daniels, Ö. Farkas, J.B. Foresman, J. V. Ortiz, J. Cioslowski, D.J. Fox, Gaussian 09, Revision D.01, (2013).
30. M.A. Abdulsattar, H.M. Abduljalil, H.H. Abed, Reaction mechanisms of pristine and Cu-doped ZnO clusters with ethanol using Evans-Polanyi principle, Emerging Materials Research. 12 (2023) 60–67. https://doi.org/10.1680/jemmr.22.00149.
31. M.A. Abdulsattar, T.H. Mahmood, H.H. Abed, H.M. Abduljalil, Adsorption and desorption of acetone by TiO2 clusters: Transition state theory and sensing analysis, ChemPhysMater. (2023). https://doi.org/10.1016/j.chphma.2023.05.001.
32. C. Corbisieri, The Logistic Function in Glass Transition Models of Amorphous Polymers: II. A Theoretical Framework for Isothermal Compression Processes, Macromolecular Theory and Simulations. 34 (2025). https://doi.org/10.1002/mats.202500052.
33. M.E. Redd, C.J. Guffey, E.L. Gustafson, E.H. Hart, K.S. McQuade, N.F. Giles, T.A. Knotts IV, W.V. Wilding, Autoignition temperature trends for various chemical families, Fuel. 355 (2024). https://doi.org/10.1016/j.fuel.2023.129321.